



Special Feature: Advanced Thermal Management Technology for Developing the High-efficiency Vehicle

Research Report

Tailoring Thermal Radiation toward Novel Thermal Devices

Kota Ito, Kazutaka Nishikawa, Atsushi Miura, Hiroshi Toshiyoshi and Hideo Iizuka

Report received on Jun. 15, 2018

■**ABSTRACT**■ Thermal radiation can be controlled by sub-wavelength structures or phase-change materials. In this review, we present six types of thermal radiation control, namely thermal rectifiers, multilevel thermal memory devices, metal-insulator-metal metamaterials, tunable thermal emitter with graphene and gratings, gap formation methodology for near-field radiative heat transfer, and near-field thermal switches. These works open pathways toward the realization of radiative thermal management systems with various functionalities.

■**KEYWORDS**■ Thermal Radiation, Phase-change Materials, Metamaterials, Subwavelength Gratings, Near-field Radiative Heat Transfer, Gap Formation Methodologies, Thermal Information Processing

1. Introduction

Thermal radiation or radiative heat transfer is one of the three principal mechanisms of heat transfer. It is mediated by the transport of electromagnetic waves, unlike the other two mechanisms, convection and conduction, each of which requires materials to transport heat. In all the materials that have finite temperature, electrons and atoms are thermally agitated, which results in electromagnetic emission to the surroundings. For example, it is well known that sunlight is thermal radiation from the sun, of which the surface temperature is around 5800 K. In everyday life, we feel thermal radiation from incandescent lamps, infrared heaters, and wood-fire ovens.

There are numbers of engineering fields where the control of thermal radiation is used to add new functionalities or improve system performance. These include thermophotovoltaics, mid-infrared light sources, and radiative cooling.

A quantized electromagnetic wave is called a photon, which has energy hc/λ , where $h = 6.63 \times 10^{-34}$ m²kg/s is the Planck constant, $c = 3.00 \times 10^8$ m/s is the speed of light, and λ is the wavelength. The hemispherical spectral emissive power from a blackbody $e_{\lambda b}$ is the function of the wavelength λ and the temperature T , and is given by Planck's law:

$$e_{\lambda b}(\lambda, T) = \frac{2\pi hc^2}{\lambda^5} \frac{1}{\exp(hc / \lambda k_B T) - 1},$$

where k_B is the Boltzmann constant.

A real body in our world is not an ideal blackbody, but has non-zero reflectance and transmittance. The ability to emit thermal radiation compared to a blackbody is defined as emissivity. Metals generally have low emissivity, while organic materials have high emissivity. One of the goals of study on thermal radiation is to control emissivity as required. Both materials research and surface structuring have been employed to achieve desired emissivity in various applications, such as thermophotovoltaics, mid-infrared light sources, and radiative cooling.

In this review, we introduce our recent works with respect to thermal radiation control. In Sec. 2, we experimentally demonstrate a thermal rectifier with vanadium dioxide. In Sec. 3, we firstly develop a multilevel thermal information storage device. In Sec. 4, we present a metal-insulator-metal metasurface with quasi-monotonic thermal emission. In Sec. 5, we theoretically discuss a thermal emitter with tunability by utilizing multilayered graphene and gratings. In Sec. 6, a method to form a nanogap for near-field radiative heat transfer is introduced. In Sec. 7, we

demonstrate a near-field radiative thermal switch. These works are summarized in Sec. 8.

2. Thermal Rectifiers

A thermal rectifier is an analog of an electrical diode, and the heat current through the rectifier is modulated according to the direction of the heat flow through it.⁽¹⁻³⁾ **Figure 1(a)** shows a schematic illustration of the proposed thermal rectifier.⁽⁴⁾ The thermal rectifier utilizes thermal radiation, which is largely modulated due to the metal-insulator transition of vanadium dioxide (VO_2). The emitter temperature T_H and the receiver temperature T_L are set so as to satisfy $T_L < 340 \text{ K} < T_H$. In the forward scenario, the VO_2 film is in the insulating state, so that the radiative flux from the fused quartz substrate is accepted by the underlying silicon substrate through the quasi-transparent VO_2 film. In the reversed scenario, the VO_2 film is in the metallic state and reflects back the thermal radiation from the silicon substrate, which results in a small radiative heat flux toward the fused quartz substrate. Note that VO_2 in the metallic state is far from a perfect electric conductor, so that a finite amount of thermal emission is transferred to the anode.

The heat flux across the thermal rectifier was measured with a receiver at 300 K using the apparatus shown in **Fig. 2**. The heat flux was measured twice while inverting the direction of the thermal rectifier, so as to evaluate both the forward and the reverse

scenarios. In the forward scenario, the heat flux increases with the emitter temperature. In the reverse scenario, the heat flux decreases in the range from 340 K to 350 K due to the phase change of VO_2 from the insulating state to the metallic state. During cooling, the heat flux returns to high values through the phase change from the metallic state to the insulating state. The transition temperature differs between heating and cooling, and this hysteresis is due to the first-order phase transition of VO_2 . Such a hysteresis was also reported in the literature.^(5,6)

3. Multilevel Thermal Memory Device

Thermal information processing is attracting broad interest as an analog of modern-VLSI (very-large scale integrated circuits) based computing. We have experimentally demonstrated a radiative thermal memory⁽⁷⁾ that utilizes the hysteretic metal-insulator transition of VO_2 . **Figure 3(a)** shows the configuration of the proposed multilevel thermal memory device. The device is composed of three parts, an emitter, a middle part, and a receiver. The measured transient response of the radiative thermal memory is shown in **Fig. 3(b)**. At first, the temperature settles to state (0) because of the insulating state of VO_2 . In the next step, the membrane was heated and the temperature settles to another state (1). The membrane was then heated again and the temperature settled to a slightly higher temperature (2). The membrane was then heated completely to realize the completely metallic state and the steady-state (3). The membrane was then cooled completely to realize state (0). This is the first report of a multi-level thermal memory. In this report, the memory stores four states, but it is generally possible to store more than four levels by utilizing

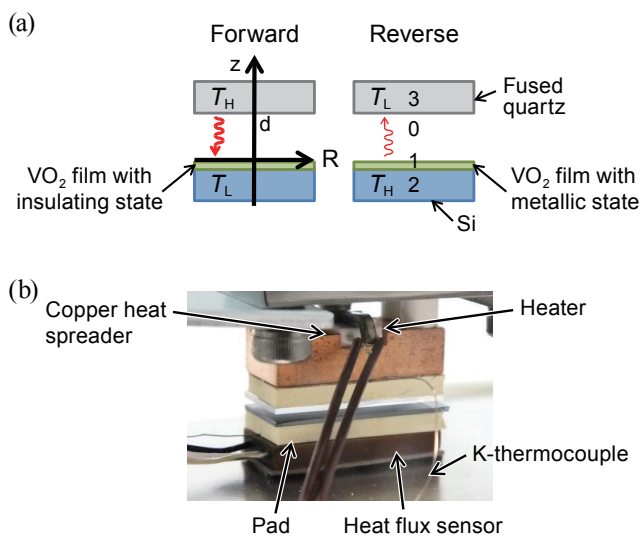


Fig. 1 Thermal rectifier. (a) Configuration. (b) Rectifier measurement system.

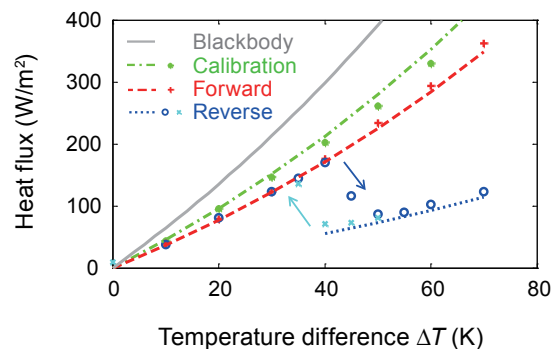


Fig. 2 Heat flux profile.

this multilevel memory. The figures show that thermal radiative heat transfer opens a new era of radiative information processing.

4. Metal-insulator-metal Metamaterial

This section demonstrates the control of parasitic electromagnetic modes excited in metal-insulator-metal metamaterials.^(8,9) **Figure 4(a)** shows a schematic illustration of conventional square metamaterial resonators. The geometrical parameters are $P = 1.96 \mu\text{m}$,

$w = l = 1.26 \mu\text{m}$, $h = 0.1 \mu\text{m}$, and $d = 0.13 \mu\text{m}$. These resonators emit at specific wavelengths and at a specific temperature of 400 K. The densely-placed square resonators shown in Fig. 4(b) emit with parameters of $P = 0.89 \mu\text{m}$, $w = l = 0.87 \mu\text{m}$, $h = 0.1 \mu\text{m}$ and $d = 0.09 \mu\text{m}$. The gap between the resonators is $0.02 \mu\text{m}$, as shown in Fig. 4(c), which enables strong interaction between the resonators.

The suppression of these modes enables quasi-monochromatic thermal emission. Suppression is performed partially due to the frequency shift of

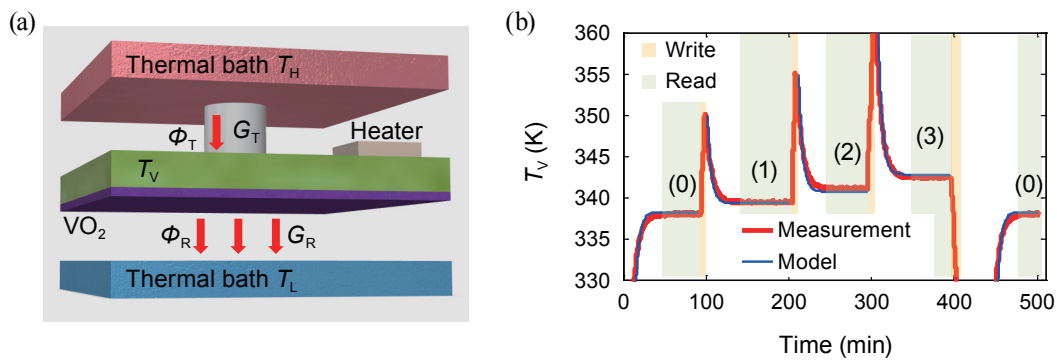


Fig. 3 Thermal memory. (a) Configuration. (b) Transient thermal response.

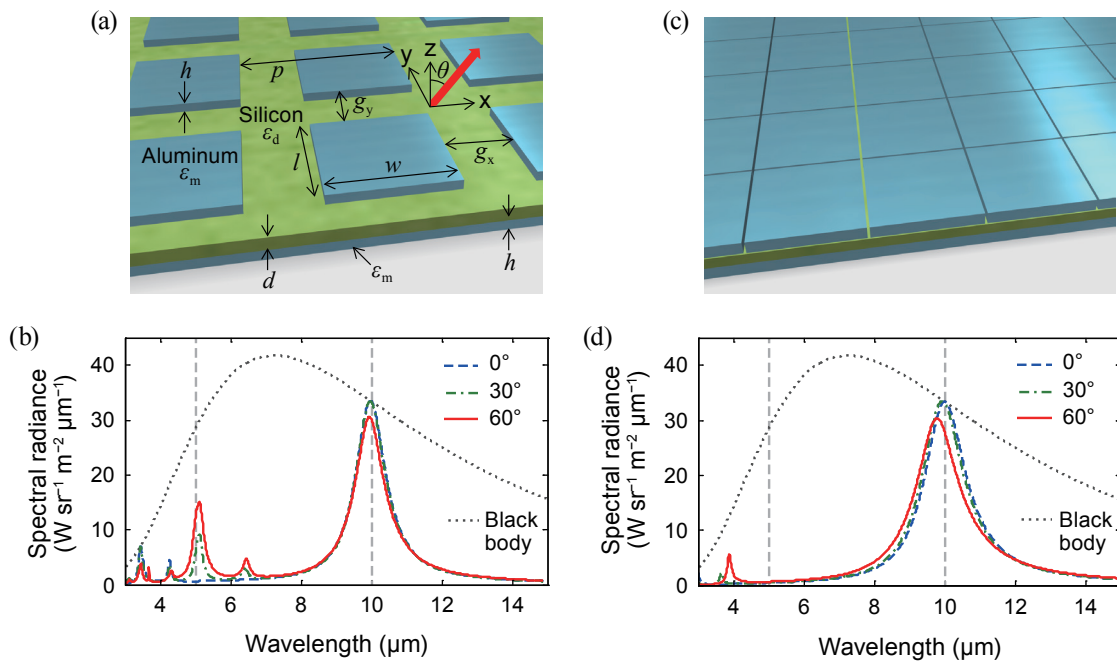


Fig. 4 Metal-insulator-metal metasurface. (a) Conventional metasurface. (b) Angularly-dependent emission spectra. (c) Densely-tiled resonators. (d) Emission from densely-tiled resonators.

the second-order resonance, which is realized by arranging the rectangular resonators in a diagonal manner,⁽¹⁰⁾ or by densely placing square resonators,⁽¹¹⁾ as shown in **Fig. 5(c)**. Figure 5(d) shows thermal emission spectra from a conventional thermal emitter. Figure 5(e) shows the thermal emission spectra from the densely-tiled resonators. The second-order resonance located around 4-5 μm is red-shifted due to the coupling between resonators. Other parasitic modes observed in conventional square resonators are successfully suppressed by dense placement. The metamaterials are fabricated as shown in Figs. 5(a), (b) and (c), and their thermal emission spectra are measured using Fourier-transformed infrared spectroscopy. The measured spectra (Figs. 5(d) and (e)) are supported by numerical simulations with CST microwave studio denoted by the blue curve. The control of the parasitic modes enables the realization of quasi-monochromatic thermal emitters.

5. Tunable Thermal Emitter with Graphene and Grating

Tunable thermal emission adds further functionality on the thermal radiation control. We demonstrate a directional thermal emission from a complex structure with gratings and graphene.⁽¹²⁾ In a previous work,

surface phonon polariton modes in a SiC grating⁽¹³⁾ and a guided mode resonance were coupled with each other to realize directional thermal emission. Surface plasmon polaritons in multilayered graphene and guided mode resonance in the grating couples to emit directional thermal emission dominantly toward one angle.⁽¹⁴⁾ **Figure 6** shows the silicon grating structure with multilayered graphene. The number of graphene layers q is chosen to reduce the lateral wavenumber of the plasmon. The pitch p of the grating is selected so as to match the lateral wavenumbers of the guided mode and the graphene plasmon at a wavelength of 10 μm . The width w and the thickness t of the grating are selected such that the guided mode resonance is excited. The height h of the grating with respect to the top graphene layer is selected to obtain sufficient coupling between the guided mode resonance and the graphene plasmon. The distance g between graphene layers and the permittivity of silicon are set to be 10 μm and 3.422, respectively. We have observed thermal emission toward the normal direction at a wavelength of 10 μm . Furthermore, a thermal emitter with beam scanning capability can be realized by changing the height of the grating and the chemical potential. In **Fig. 7**, the emission angle is swept from the normal direction to the oblique direction using the coupling between the guided mode resonance in the

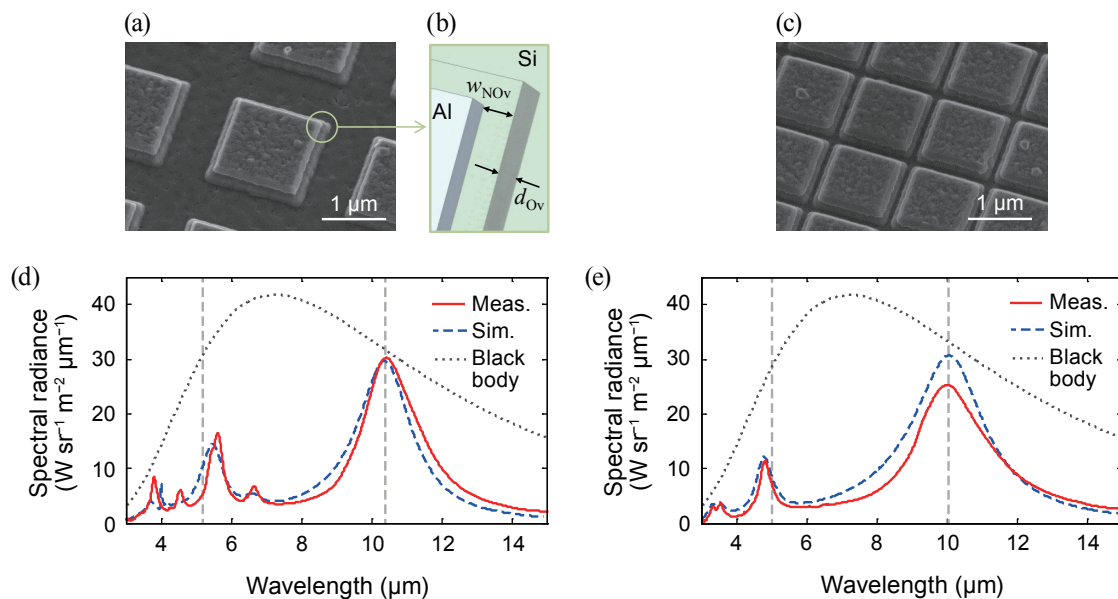


Fig. 5 Experimentally fabricated metal-insulator-metal metasurface. (a) Conventional metasurface. (b) Zoomed-up view utilized in simulations. (c) Densely-tiled resonators. (d) Emission from conventional resonators. (e) Emission from densely-tiled resonators.

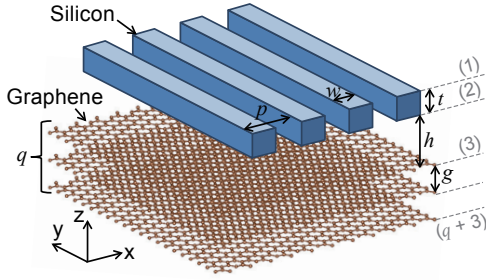


Fig. 6 Silicon grating positioned above multilayered graphene. The structure is periodic in the x-direction and is infinite in the y-direction. The illustration is not to scale. The region numbers are shown in gray.

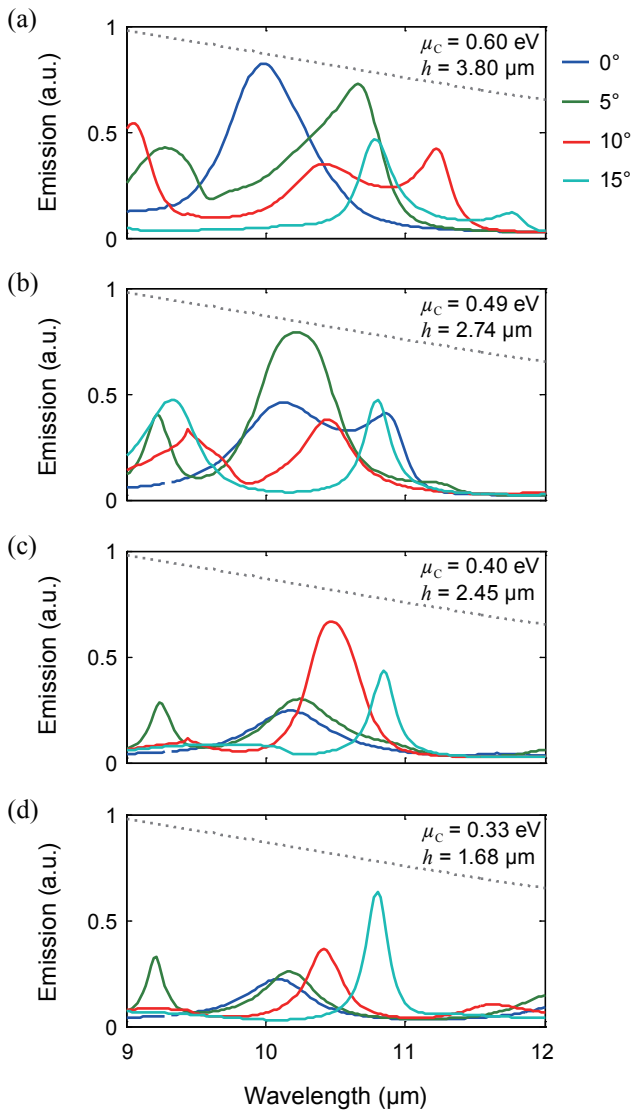


Fig. 7 Emissivity profiles while concurrently tuning the chemical potential of the graphene layers and the grating height. The chemical potential and the grating height were set to induce directional emission toward (a) 0° (b) 5° (c) 10° and (d) 15°. The gray dotted curves denote the blackbody limit.

grating and the graphene plasmon. The emission angle is then swept from the normal direction to oblique angles, by changing the chemical potential from 0.60 eV to 0.49 eV, 0.40 eV, and 0.33 eV, and changing the grating height from 3.80 μm to 2.74 μm, 2.45 μm, and 1.68 μm to achieve thermal emission to 0°, 5°, 10°, and 15°. This emission is swept from the normal direction and the resonant wavelength is set at 10 μm.

6. Near-field Radiative Heat Transfer

The amount of the radiative heat transfer is limited by the Stefan-Boltzmann law in the far-field regime where the distance between the hot body and the cold body is sufficiently larger than the Wien peak wavelength. On the other hand, the radiative transfer between two materials placed in proximity is no more explained by Planck’s law or the concept of emissivity.^(15,16) Under certain conditions, the radiative transfer is larger than the blackbody radiation calculated by the Stefan-Boltzmann law. This heat flux enhancement due to near-field coupling is called near-field radiative heat transfer or near-field thermal radiation. Near-field radiative heat transfer from a hot semi-infinite plate with a temperature T_H to a cold semi-infinite plate with a temperature T_L across a planar gap d is calculated as follows:

$$\phi = \frac{1}{\pi^2} \int_0^{+\infty} d\omega \left[\Theta(\omega, T_H) - \Theta(\omega, T_L) \right] \sum_{j=s,p} \int_0^{+\infty} Z(\omega, \beta, j) \beta d\beta, \quad (1)$$

where the exchange function $Z(\omega, \beta, j)$ is

$$\int_0^{+\infty} Z(\omega, \beta, j) \beta d\beta = \int_0^{\omega/c} \frac{(1 - |r_j|^2)^2}{4|1 - r_j^2 e^{2i\gamma_0 d}|^2} \beta d\beta + \int_{\omega/c}^{+\infty} \frac{\text{Im}(r_j)^2 e^{-2\text{Im}(\gamma_0) d}}{|1 - r_j^2 e^{-2\text{Im}(\gamma_0) d}|^2} \beta d\beta, \quad (2)$$

where ω is the frequency, c is the speed of light, β is the lateral wavenumber, j is the polarization, $\Theta(\omega, T) = \hbar\omega / (\exp(\hbar\omega/k_B T) - 1)$ is the mean energy of the Planck oscillator at temperature T , k_B is the Boltzmann constant, \hbar is the reduced Planck constant, r_j is the Fresnel reflection coefficient incident from the vacuum to the plate in j -polarization, and γ_0 is the wavenumber perpendicular to the plate surface

in the gap. Thermal radiative transfer between bodies is divided into two parts, i.e., far-field transfer and near-field heat transfer.

A submicron gap formation methodology for near-field radiative heat transfer is presented in this section.⁽¹⁷⁾ The spacers were fabricated using a standard microfabrication process. Two processes, deep-ultraviolet contact lithography and buffered hydrofluoric acid (BHF) etching, were utilized for fabrication. Deep-ultraviolet contact lithography was utilized to transfer the spacer pattern from the photomask to the photoresist on a fused quartz substrate. Positive photoresist iP3100 (TOK) and developer NMD-3 (TOK) were employed. **Figure 8** shows SEM images of the spacers.

The apparatus shown in **Fig. 9(a)** was developed to achieve three functionalities required for this work, i.e., the exertion of force, evaluation of the gap uniformity, and measurement of the heat transfer. For the exertion of force, a copper heat spreader was connected to a compression spring through ceramic posts. The

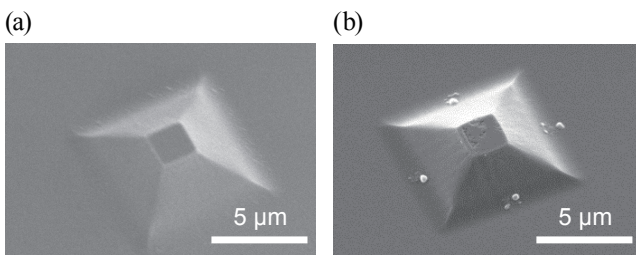


Fig. 8 SEM image of spacer pillars.

compression spring has a small spring constant of 1.0 N/mm, which enables precise control of the applied force. For soft gap formation, two extension springs with a smaller spring constant of 0.06 N/m were connected in parallel to the compression spring. The copper heat spreader was perforated at four points to allow the thin optical fiber access to the chips. After gap formation, an optical fiber was inserted to each hole sequentially for the reflectance measurement.

The gap formation and heat transfer measurement were repeated four times for each nominal gap of 0.5 μm , 1.0 μm , and 2.0 μm . The measured heat transfer coefficients are shown in **Fig. 9(b)**. The standard deviation of the optical interferometry at each of the four points is shown as the error bar in the x-direction, and that of the heat flux measurement is shown in the y-direction. The theoretically calculated radiative heat transfer is plotted as solid lines, while twice the theoretical heat flux is plotted as dashed lines.

The measured flux is equal to or smaller than twice the theoretical flux, which means that the parasitic heat conduction through the spacers was successfully suppressed to be equal to or smaller than the electromagnetic heat transfer. This suppression of the parasitic heat conduction is achieved by the presented gap formation methodology with the appropriate spacer design.

7. Near-field Radiative Thermal Switch

Dynamic control of heat transfer in solid-state systems enables the possibility of intelligent thermal

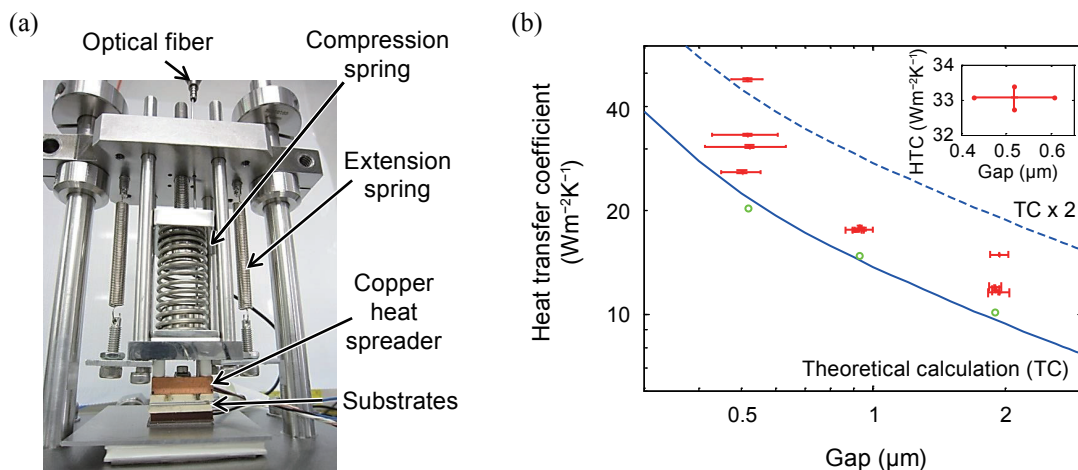


Fig. 9 (a) Heat flux measurement apparatus. (b) Heat transfer coefficients of the gaps.

management in nanoscale systems.⁽¹⁸⁾ We have experimentally confirmed that the radiative heat transfer is actively modulated beyond the blackbody limit.⁽¹⁹⁾ The near-field electromagnetic heat transfer through phonon-polariton coupling is actively controlled by the phase-change of tungsten-doped VO₂. The functionalized heat flux is transferred over an area of 1.6 cm² across a 370 nm gap, which is maintained by the microfabricated spacers and the applied pressure (**Fig. 10(a)**). The uniformity of the formed gap was confirmed by optical interferometry, and the measured heat transfer is well explained as the sum of the radiative and parasitic conductive components. Active modulation of the radiative heat flux across a 370 nm gap was demonstrated, as shown in Fig. 10(b). Initially, T_H and T_L were set at 355 K and 295 K, respectively, and the VO₂ film remained insulating (0-100 min). T_H and T_L were then

respectively changed to 385 K and 325 K to bring the VO₂ film into the metallic phase (170-290 min). The temperature difference $T_H - T_L$ was maintained under both conditions. The heat flux across the gap was significantly suppressed when VO₂ is in the metallic phase. The heat flux also recovers when the temperature profile is set back to the original (400-530 min). Note that the bold blue curve corresponds to the steady-state temperature conditions. The methodology presented to form a nanoscale gap with functionalized heat flux will enable smart thermal management in various scenarios, ranging from highly integrated systems to macroscopic apparatus.

8. Summary

We have introduced various types of thermal devices, including a thermal rectifier with vanadium dioxide, multilevel thermal information storage device, a metal-insulator-metal metasurface with quasi-monochromatic thermal emission, a thermal emitter with tunability by utilizing multilayered graphene and gratings, a method to form a nanogap for near-field radiative heat transfer, and a near-field radiative thermal switch with vanadium dioxide. These devices are enabled by sub-wavelength structures or phase-change materials and are expected to pave the way toward a new era of thermal radiation control.

References

- (1) Chang, C. W., Okawa, D., Majumdar, A. and Zettl, A., "Solid-state Thermal Rectifier", *Science*, Vol. 314, No. 5802 (2006), pp. 1121-1124.
- (2) Kobayashi, W., Teraoka, Y. and Terasaki, I., "An Oxide Thermal Rectifier", *Appl. Phys. Lett.*, Vol. 95, No. 17 (2009), 171905.
- (3) Sawaki, D., Kobayashi, W., Morimoto, Y. and Terasaki, I., "Thermal Rectification in Bulk Materials with Asymmetric Shape", *Appl. Phys. Lett.*, Vol. 98, No. 8 (2011), 081915.
- (4) Ito, K., Nishikawa, K., Iizuka, H. and Toshiyoshi, H., "Experimental Investigation of Radiative Thermal Rectifier Using Vanadium Dioxide", *Appl. Phys. Lett.*, Vol. 105, No. 25 (2014), 253503.
- (5) Kats, M. A., Sharma, D., Lin, J., Genevet, P., Blanchard, R., Yang, Z., Qazilbash, M. M., Basov, D. N., Ramanathan, S. and Capasso, F., "Ultra-thin Perfect Absorber Employing a Tunable Phase Change Material", *Appl. Phys. Lett.*, Vol. 101, No. 22 (2012), 221101.

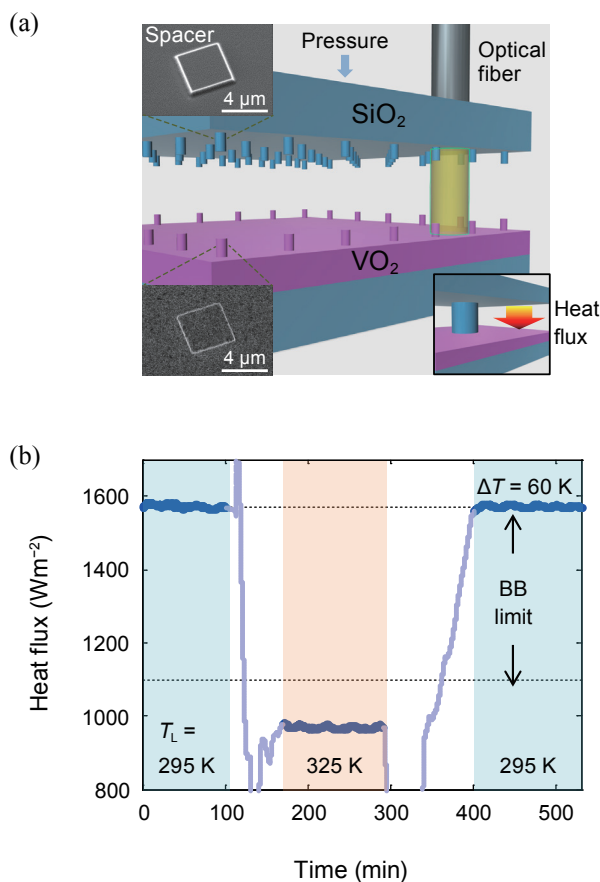


Fig. 10 Dynamic heat modulation across the nanogap.
 (a) Nanoscale gap formation methodology.
 (b) Heat transfer across the gap with different temperature bias.

- (6) Kats, M. A., Blanchard, R., Zhang, S., Genevet, P., Ko, C., Ramanathan, S. and Capasso, F., “Vanadium Dioxide as a Natural Disordered Metamaterial: Perfect Thermal Emission and Large Broadband Negative Differential Thermal Emittance”, *Phys. Rev. X*, Vol. 3, No. 4 (2013), 041004.
- (7) Ito, K., Nishikawa, K. and Iizuka, H., “Multilevel Radiative Thermal Memory Realized by the Hysteretic Metal-insulator Transition of Vanadium Dioxide”, *Appl. Phys. Lett.*, Vol. 108, No. 5 (2016), 053507.
- (8) Lee, B. J., Wang, L. P. and Zhang, Z. M., “Coherent Thermal Emission by Excitation of Magnetic Polaritons between Periodic Strips and a Metallic Film”, *Optics Express*, Vol. 16, No. 15 (2008), pp. 11328-11336.
- (9) Liu, X., Tyler, T., Starr, T., Starr, A. F., Jokerst, N. M. and Padilla, W. J., “Taming the Blackbody with Infrared Metamaterials as Selective Thermal Emitters”, *Phys. Rev. Lett.*, Vol. 107, No. 4 (2011), 045901.
- (10) Ito, K., Toshiyoshi, H. and Iizuka, H., “Metal-insulator-metal Metamaterial Absorbers Consisting of Proximity-coupled Resonators with the Control of the Fundamental and the Second-order Frequencies”, *J. Appl. Phys.*, Vol. 119, No. 6 (2016), 063101.
- (11) Ito, K., Toshiyoshi, H. and Iizuka, H., “Densely-tiled Metal-insulator-metal Metamaterial Resonators with Quasi-monochromatic Thermal Emission”, *Optics Express*, Vol. 24, No. 12 (2016), pp. 12803-12811.
- (12) Ito, K. and Iizuka, H., “Directional Thermal Emission Control by Coupling between Guided Mode Resonances and Tunable Plasmons in Multilayered Graphene”, *J. Appl. Phys.*, Vol. 120, No. 16 (2016), 163105.
- (13) Wang, S. S. and Magnusson, R., “Theory and Applications of Guided-mode Resonance Filters”, *Appl. Optics*, Vol. 32, No. 14 (1993), pp. 2606-2613.
- (14) Ito, K., Matsui, T. and Iizuka, H., “Thermal Emission Control by Evanescent Wave Coupling Between Guided Mode of Resonant Grating and Surface Phonon Polariton on Silicon Carbide Plate”, *Appl. Phys. Lett.*, Vol. 104, No. 5 (2014), 051127.
- (15) Ottens, R. S., Quetschke, V., Wise, S., Alemi, A. A., Lundock, R., Mueller, G., Reitze, D. H., Tanner, D. B. and Whiting, B. F., “Near-field Radiative Heat Transfer between Macroscopic Planar Surfaces”, *Phys. Rev. Lett.*, Vol. 107, No. 1 (2011), 014301.
- (16) Kim, K., Song, B., Fernández-Hurtado, V., Lee, W., Jeong, W., Cui, L., Thompson, D., Feist, J., Reid, M. T. H., García-Vidal, F. J., Cuevas, J. C., Meyhofer, E. and Reddy, P., “Radiative Heat Transfer in the Extreme Near Field”, *Nature*, Vol. 528 (2015), pp. 387-391.
- (17) Ito, K., Miura, A., Iizuka, H. and Toshiyoshi, H., “Parallel-plate Submicron Gap Formed by Micromachined Low-density Pillars for Near-field Radiative Heat Transfer”, *Appl. Phys. Lett.*, Vol. 106, No. 8 (2015), 083504.
- (18) Ihlefeld, J. F., Foley, B. M., Scrymgeour, D. A., Michael, J. R., McKenzie, B. B., Medlin, D. L., Wallace, M., Trolier-McKinstry, S., Hopkins, P. E., “Room-temperature Voltage Tunable Phonon Thermal Conductivity via Reconfigurable Interfaces in Ferroelectric Thin Films”, *Nano Lett.*, Vol. 15, No. 3 (2015), pp. 1791-1795.
- (19) Ito, K., Nishikawa, K., Miura, A., Toshiyoshi, H. and Iizuka, H., “Dynamic Modulation of Radiative Heat Transfer beyond the Blackbody Limit”, *Nano Lett.*, Vol. 17, No. 7 (2017), pp. 4347-4353.

Figs. 1-2

Reprinted from *Appl. Phys. Lett.*, Vol. 105, No. 25 (2014), 253503, Ito, K., Nishikawa, K., Iizuka, H. and Toshiyoshi, H., Experimental Investigation of Radiative Thermal Rectifier Using Vanadium Dioxide, © 2014 AIP, with permission from AIP Publishing LLC.

Fig. 3

Reprinted from *Appl. Phys. Lett.*, Vol. 108, No. 5 (2016), 053507, Ito, K., Nishikawa, K. and Iizuka, H., Multilevel Radiative Thermal Memory Realized by the Hysteretic Metal-insulator Transition of Vanadium Dioxide, © 2016 AIP, with permission from AIP Publishing LLC.

Figs. 4-5

Reprinted from *Optics Express*, Vol. 24, No. 12 (2016), pp. 12803-12811, Ito, K., Toshiyoshi, H. and Iizuka, H., Densely-tiled Metal-insulator-metal Metamaterial Resonators with Quasi-monochromatic Thermal Emission, © 2016 OSA.

Figs. 6-7

Reprinted from *J. Appl. Phys.*, Vol. 120, No. 16 (2016), 163105, Ito, K. and Iizuka, H., Directional Thermal Emission Control by Coupling Between Guided Mode Resonances and Tunable Plasmons in Multilayered Graphene, © 2016 AIP, with permission from AIP Publishing LLC.

Figs. 8-9

Reprinted from *Appl. Phys. Lett.*, Vol. 106, No. 8 (2015), 083504, Ito, K., Miura, A., Iizuka, H. and Toshiyoshi, H., Parallel-plate Submicron Gap Formed by Micromachined Low-density Pillars for Near-field Radiative Heat Transfer, © 2015 AIP, with permission from AIP Publishing LLC.

Fig. 10

Reprinted from Nano Lett., Vol. 17, No. 7 (2017), pp. 4347-4353, Ito, K., Nishikawa, K., Miura, A., Toshiyoshi, H. and Iizuka, H., Dynamic Modulation of Radiative Heat Transfer beyond the Blackbody Limit, © 2017 ACS, with permission from American Chemical Society.

Kota Ito

Research Fields:

- Nanophotonics
- Nanoscale Heat Transfer

Academic Degree: Ph.D.

Academic Societies:

- The Japan Society of Applied Physics
- The Institute of Electrical Engineers of Japan
- The Heat Transfer Society of Japan

**Kazutaka Nishikawa**

Research Fields:

- Functional Materials
- Thin Films
- Optics

Academic Society:

- The Japan Society of Applied Physics

**Atsushi Miura**

Research Field:

- Microfabrication

Academic Society:

- The Japan Society of Applied Physics

**Hiroshi Toshiyoshi***

Research Field:

- Micro Electro Mechanical Systems

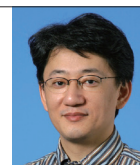
Academic Degree: Ph.D.

Academic Societies:

- The Japan Society of Applied Physics
- The Institute of Electrical Engineers of Japan
- The Institute of Electronics, Information and Communication Engineers
- IEEE

Awards:

- Marubun Research Award, Marubun Research Promotion Foundation, 2008
- Electronics Society Award, IEICE, 2010
- Distinguished Paper Award, IEEJ, 2015
- Inoue Harushige Prize, Inoue Harushige Prize Committee, 2018
- Nagamori Awards, Nagamori Foundation, 2018

**Hideo Iizuka**

Research Field:

- Electromagnetic Analysis

Academic Degree: Dr.Eng.

Academic Societies:

- IEEE
- The Optical Society of America



*The University of Tokyo